

Signal Reconstruction from Quantized Noisy Samples of the Discrete Fourier Transform

Mohak Goyal and Animesh Kumar

Department of Electrical Engineering, Indian Institute of Technology Bombay, India
goyalmohak2@gmail.com, animekum@outlook.com

Abstract—In this paper, we present two variations of an algorithm for signal reconstruction from one-bit or two-bit noisy observations of the discrete Fourier transform (DFT). The one-bit observations of the DFT correspond to the sign of its real part, whereas, the two-bit observations of the DFT correspond to the signs of both the real and imaginary parts of the DFT. We focus on images for analysis and simulations, thus using the sign of the 2D-DFT. This choice of the class of signals is inspired by previous works on this problem. For our algorithm, we show that the expected mean squared error (MSE) in signal reconstruction is asymptotically proportional to the inverse of the sampling rate. The samples are affected by additive zero-mean noise of known distribution. We solve this signal estimation problem by designing an algorithm that uses contraction mapping, based on the Banach fixed point theorem. Numerical tests with four benchmark images are provided to show the effectiveness of our algorithm. Various metrics for image reconstruction quality assessment such as PSNR, SSIM, ESSIM, and MS-SSIM are employed. On all four benchmark images, our algorithm outperforms the state-of-the-art in all of these metrics by a significant margin.

Index Terms—Denoising, single-bit sampling, contraction mapping, companding, quantization, image processing.

I. INTRODUCTION

Signal reconstruction from partial information of its Fourier transform (FT) has been of interest since a long time, both for its practical applications and for its fundamental understanding [1]. Two well-known types of problems in this class are the phase retrieval and magnitude retrieval problems [1], [2]. The phase retrieval problem is the reconstruction or estimation of a signal from its FT magnitude information. It has applications in areas such as electron microscopy [3] and X-ray crystallography [4]. Recent developments in phase retrieval include its formulation as a semi-definite program with robustness guarantees by Candès, Strohmer, and Vershynina [5]. Huang, Eldar, and Sidiropoulos [6] gave a polynomial time algorithm with uniqueness and optimality guarantees for the phase retrieval problem. Phase retrieval from one-bit measurements of the magnitude has been studied in [7] and [8], among others.

The magnitude retrieval problem is the reconstruction of a signal from partial information of its FT phase. Its applications are in situations where the signal is distorted by a zero-phase blurring or point-spread function. In such cases the magnitude information is lost but the phase is retained. Li and Kurkjian

[9] showed that magnitude retrieval can be used to solve some problems in arrival-time estimation. An interesting version of the magnitude retrieval problem is the case where only coarsely quantized readings of the FT phase of the signal are available. The signal reconstruction problem with one-bit readings of FT phase has also been studied. Curtis, Oppenheim, and Lim showed that most two-dimensional signals can be reconstructed to within a scale factor from only one bit of 2D-DFT phase [10]. They presented an iterative algorithm which consists of projection onto the support region in the spatial domain and enforcement of phase information in the frequency domain. Tang, Yuan, and Wang presented an improvement to this algorithm with a specified histogram constraint [11].

Lyuboshenko and Akhmetshin studied signal reconstruction with noisy FT phase [12]. They proposed global and local regularization based reconstruction algorithms. Working on signal reconstruction with noisy FT phase, Thomas and Hayes proposed algorithms which incorporate side information such as a bound on the noise and the 2D-DFT magnitudes [13]. However, these works considered full-precision measurements only. Unlike these previous works, in this paper we consider the signal reconstruction problem with two deficiencies in the available information of the FT: (1) the recordings are corrupted with additive zero-mean noise, and (2) the recordings are quantized with precision of only one or two bits.

Signal reconstruction from coarsely quantized samples is well known in classical signal processing [14]–[19] and is particularly appealing in hardware implementations. The quantizer to one-bit is a comparator to zero and is quite fast, thus enabling high sampling rates. Dealing with one-bit recordings in the time (or spatial) domain, Kumar and Prabhakaran obtained a mean squared error of $O(1/K)$ for (classically) bandlimited signals with K being the oversampling factor with respect to the Nyquist rate [18]. Cvetkovič, Daubechies, and Logan considered the case of irregular sampling and used a deterministic dither, obtaining a $O(1/K)$ pointwise error [19]. Khobahi et. al. have employed deep neural networks for one-bit signal recovery [20]. The application of one-bit samples for channel estimation has been explored in [21] and [22], among others. Another application of one-bit quantization has been shown in graph signal processing for bandlimited graph signals by Goyal and Kumar [23].

Compressed sensing with one-bit samples was introduced by Boufounos and Baraniuk [24]. They gave a convex relaxation of the problem, employing a one-sided quadratic penalty. Zymnis, Boyd, and Candès gave two algorithms for com-

Most of this work was done when Mohak Goyal was with the Department of Electrical Engineering at IIT Bombay. He is now with the Department of Management Science & Engineering at Stanford University.

pressed sensing with one-bit samples, based on l_1 regularised least squares and l_1 regularised maximum likelihood [25]. Xu and Jacques proposed an algorithm that utilizes a random dither [26] for one-bit compressed sensing. Jacques et. al., gave the binary iterative hard thresholding (BIHT) algorithm which is also robust to noise [27]. For noiseless signals, Friedlander et al. proved that a variant of BIHT achieves the optimal $O(1/K)$ error decay rate with high probability [28]. We use the BIHT algorithm as a baseline while evaluating the performance of our algorithm.

Boufounos introduced angle-preserving quantized phase embeddings [29]. They consider a real valued signal, for which phase measurements were obtained through a complex linear transform. They showed that these embeddings generalize the binary epsilon stable embeddings in the same sense that the phase of complex numbers generalizes the sign of real numbers. Boufounos introduced complex compressive sensing where measurements of a sparse signal are obtained via a complex, fat sensing matrix [30]. They proved that with complex Gaussian random sensing matrices, one can estimate the direction of such a signal from the phase of the compressive measurements. Jacques and Feuillen extended this idea to any signals belonging to a symmetric, low-complexity conic set of reduced dimensionality, including the set of sparse signals or the set of low-rank matrices [31]. These works consider only noiseless signals.

In this work, we consider the problem of signal estimation from noisy quantized readings of the DFT. With regard to quantization, we restrict our attention to one-bit or two-bit precision only. The one-bit observations of the DFT correspond to the sign of its real part, whereas, the two-bit observations of the DFT correspond to the signs of both the real and imaginary parts of the DFT. Similar to Kumar and Prabhakaran in [18], we provide a Banach contraction mapping based algorithm for estimation and denoising. Unlike their work, the algorithm we present can also be used to estimate non-bandlimited signals.

Our algorithm achieves the optimal $O(1/K)$ error decay rate. This rate has also been observed by other signal reconstruction approaches, for example in linear regression [32], with quantized samples [18], [19], [33], and in compressed sensing [34], [35]. While there exists literature on compressed sensing with one-bit samples, (see e.g., [24]–[28], [34], [35]) there has not been much work on denoising of ‘lowpass’ signals from noise affected and single-bit quantized samples. Thus, there is significant difference in the signal model (lowpass versus sparse), presence or absence of noise, and guarantees (analytical results versus recovery algorithms with simulations) between this work and the compressed sensing literature. We sample only the sign of the real and imaginary parts of the noisy DFT, and use the distribution of the noise to perform signal reconstruction with $O(1/K)$ error decay rate.

There are two variations of the algorithm we present. Algorithms 1 and 2 solve the signal reconstruction problem with one-bit and two-bit recordings respectively. We use Banach’s contraction mapping theorem to prove that our algorithm converges to a unique point. We also provide a proof of the decay of the expected mean squared error (MSE) for our algorithm with increase in sampling rate. It is inversely

proportional to the sampling rate. In this paper we consider grayscale images. We demonstrate the results on the IEEE logo image, the Lena image, the cameraman image, and the peppers image. We also show comparisons with two current algorithms.

Paper outline: The problem setup is described in Section II. The algorithms are given in Section III. In Section IV, bounds on the estimation error are given with proofs. Simulations and their results are explained in Section V. Conclusions are drawn in Section VI.

Notation: We use standard notation: the set of real numbers is denoted by \mathbb{R} , the complex numbers by \mathbb{C} , the 2D-discrete Fourier transform (2D-DFT) of the real image $g[n_1, n_2]$ is denoted by $\tilde{g}[k_1, k_2]$. The indicator function, denoted by $\mathbb{1}(x > 0)$, takes value 1 if $x > 0$ and 0 otherwise. The Frobenius norm and the max norm of matrix \mathcal{M} are given by $\|\mathcal{M}\|_F$ and $\|\mathcal{M}\|_{\max}$ respectively. The transpose of matrix \mathcal{M} is denoted by \mathcal{M}^T . The complex conjugate of c is denoted by c^* . The vectorization operation on a matrix corresponds to concatenating its columns in order. The vectorized form of matrix $\mathcal{M} \in \mathbb{C}^{N \times N}$ is denoted by the vector $\mathcal{M}^v \in \mathbb{C}^{N^2}$. The 2D-DFT operator is denoted by $\mathfrak{F}(\cdot)$ such that $\tilde{g}[k_1, k_2] = \mathfrak{F}(g[n_1, n_2])$ and the inverse 2D-DFT (2D-IDFT) operator is denoted by $\mathfrak{F}^{-1}(\cdot)$ such that $g[n_1, n_2] = \mathfrak{F}^{-1}(\tilde{g}[k_1, k_2])$.

II. SIGNAL AND SAMPLING MODEL

We consider grayscale images. As is natural for images, we consider that the signal value at any pixel is in the interval $[0, 255]$. The sampling is done in the frequency domain. Let the image $g[n_1, n_2]$ be of $M \times M$ dimension. The 2D-DFT is computed such that there are $N \times N$ samples in the 2D-DFT of $g[n_1, n_2]$, i.e., in $\tilde{g}[k_1, k_2]$. We ensure that $N > 2M$ such that the real part of 2D-DFT is sufficient to reconstruct the image [36]. Denote the noise affecting the real and imaginary parts by $W_R[k_1, k_2]$ and $W_I[k_1, k_2]$ respectively. For the noise model, we have the following assumption:

Assumption 1. *The real and imaginary parts of the 2D-DFT are affected by independent additive zero-mean noise of a known distribution, which is symmetric w.r.t. 0.*

Additional additive white Gaussian noise (AWGN) of variance σ_d^2 is added to dither the signal if the noise distribution doesn’t have mass over the entire region withing the bounds of the signal. This is required since the proposed algorithm depends on the presence of noise of known distribution to be able to recover the signal. This requirement is satisfied by adding the dither noise. The MLE based algorithm of Bahmani, Boufounos, and Raj would also require noise to be present, they handle it by heuristically modifying the cost function when there is no noise [37].

Dither $d_R[k_1, k_2]$ and $d_I[k_1, k_2]$ are added to the real and imaginary parts of the 2D-DFT respectively. The use of dithering with quantized signals is well known [38]. In our model, dither is added to ensure that there is sufficient variance in the samples, and the magnitude information is captured in it. The use of dither is further discussed in Section IV-C. In our sampling model, as shown in Fig. 1,

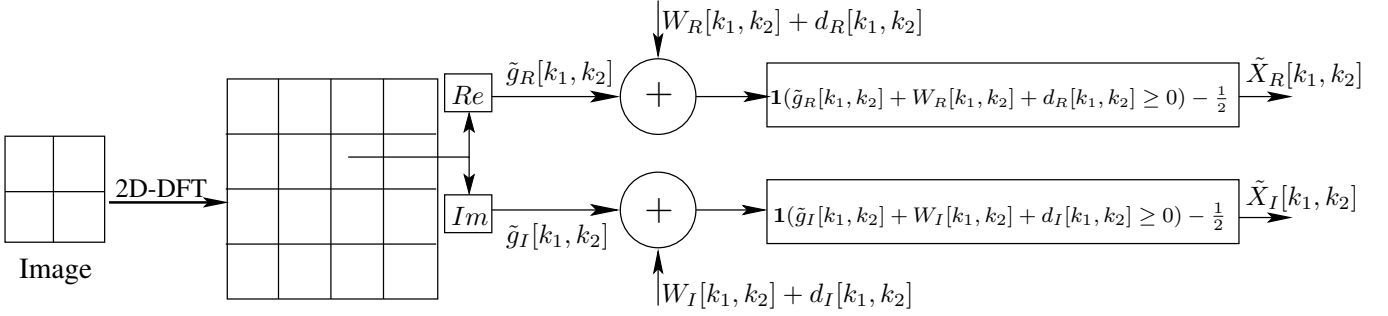


Fig. 1: The sampling scheme for our reconstruction problem. The 2D-DFT of the image has additive zero-mean noise, $W_R[k_1, k_2]$ and $W_I[k_1, k_2]$, in its real and imaginary parts respectively. AWGN dither $d_R[k_1, k_2]$ and $d_I[k_1, k_2]$ are also added. One bit each of the real and imaginary parts of the noisy 2D-DFT are recorded via a comparator with 0.

one-bit samples $\tilde{X}_R[k_1, k_2]$ and $\tilde{X}_I[k_1, k_2]$, of the real part, $\tilde{g}_R[k_1, k_2]$, and imaginary part, $\tilde{g}_I[k_1, k_2]$, respectively of the 2D-DFT, $\tilde{g}[k_1, k_2]$, are recorded as follows:

$$\tilde{X}_R[k_1, k_2] = \mathbb{1}(\tilde{g}_R[k_1, k_2] + W_R[k_1, k_2] + d_R[k_1, k_2] > 0) - \frac{1}{2}, \quad (1)$$

$$\tilde{X}_I[k_1, k_2] = \mathbb{1}(\tilde{g}_I[k_1, k_2] + W_I[k_1, k_2] + d_I[k_1, k_2] > 0) - \frac{1}{2}. \quad (2)$$

Due to conjugate symmetry of the 2D-DFT of real signals, we need to sample only half of the entries of $\tilde{X}_R[k_1, k_2]$ and $\tilde{X}_I[k_1, k_2]$. It must be noted that Algorithm 2 uses both $\tilde{X}_R[k_1, k_2]$ and $\tilde{X}_I[k_1, k_2]$, i.e., two bits of the noisy 2D-DFT. Whereas, Algorithm 1 uses only $\tilde{X}_R[k_1, k_2]$ i.e., only one bit of the noisy 2D-DFT of the image.

Recall that the 2D-DFT of $g \in \mathbb{C}^{N \times N}$ is given by:

$$\tilde{g}[k, l] = \sum_{n_1=0}^{N-1} \sum_{n_2=0}^{N-1} g[n_1, n_2] \exp\left(-j2\pi\left(\frac{kn_1}{N} + \frac{ln_2}{N}\right)\right). \quad (3)$$

Whereas, the 2D-IDFT of $\tilde{g} \in \mathbb{C}^{N \times N}$ is given by:

$$g[k, l] = \frac{1}{N^2} \sum_{n_1=0}^{N-1} \sum_{n_2=0}^{N-1} \tilde{g}[n_1, n_2] \exp\left(j2\pi\left(\frac{kn_1}{N} + \frac{ln_2}{N}\right)\right). \quad (4)$$

In the following section we give the two variations of the proposed algorithm, i.e., Algorithms 1 and 2.

III. PROPOSED SIGNAL RECONSTRUCTION ALGORITHM

In Subsection III-A we discuss Algorithm 1, which uses one-bit recordings of the 2D-DFT.

A. Using one-bit recordings of the noisy 2D-DFT phase

Recall that $\tilde{X}_R[k_1, k_2]$ is the real part of $\tilde{X}[k_1, k_2]$ and is recorded according to sampling model (1). Define the following subset of the set of real numbers, $\mathbb{S} := [-255N^2, 255N^2]$. Let operator $\mathcal{P} : \mathbb{S}^{N \times N} \rightarrow \mathbb{S}^{N \times N}$ be defined as:

$$\mathcal{P}(\tilde{g}) := \mathfrak{F}(\text{CLIP}(\text{PROJ}(\mathfrak{F}^{-1}(\tilde{g}))))). \quad (5)$$

See that operator \mathcal{P} performs a series of four operations on the frequency domain input. First it computes a 2D-DFT to convert the argument to the spatial domain. Then it sets the pixels corresponding to the zero-padding to zero. This operation is denoted by PROJ. Then it clips the pixel values to the range $[0, 255]$, i.e., it changes the entries that are greater than 255 to 255, and that are less than 0 to 0. This operation is denoted by CLIP. Finally it takes the 2D-DFT of the spatial domain image to obtain the frequency domain image. The CLIP operation ensures that $\mathcal{P}(\tilde{g})$ is in $\mathbb{S}^{N \times N}$ for all \tilde{g} in $\mathbb{S}^{N \times N}$. Notice that every operation within \mathcal{P} is a projection operation and therefore, \mathcal{P} performs a projection operation. By the property of projection operations, \mathcal{P} is non-expansive with respect to the Frobenius norm. We call this the NON-EXPANSIVE property of \mathcal{P} .

Let the map $\mathcal{T} : \mathbb{S}^{N \times N} \rightarrow \mathbb{S}^{N \times N}$ be defined as:

$$\mathcal{T}(\tilde{g}) := \mathcal{P}\left(\gamma \tilde{X}_R + \tilde{g} - \gamma\left(\mathcal{F}(\tilde{g}) - \frac{1}{2}\right)\right), \quad \tilde{g} \in \mathbb{S}^{N \times N} \quad (6)$$

$$\gamma \in \left(0, \frac{2}{f_{\max}}\right). \quad (7)$$

The function $\mathcal{F} : \mathbb{R}^{N \times N} \rightarrow \mathbb{R}^{N \times N}$ is the cumulative distribution function (CDF) of the noise (including dither), applied element-wise on the argument. Similarly, function $f : \mathbb{R}^{N \times N} \rightarrow \mathbb{R}^{N \times N}$ is the probability distribution function (PDF) of the noise, applied element-wise on the argument. The constant f_{\max} is the maximum value of the noise PDF for x in the region within the bounds of the signal. Condition (7) on parameter γ is required to ensure that $\mathcal{T}(\tilde{g})$ is a contraction mapping, w.r.t. to the Frobenius norm i.e., it reduces the Frobenius norm of the difference with the fixed point of the mapping. The one-bit of the 2D-DFT i.e., the sign of the real part of the 2D-DFT is recorded in $\tilde{X}_R[k_1, k_2]$ according to the sampling model (1).

It must be noted that the 2D-IDFT of the real part of the 2D-DFT gives two copies of the image if appropriate zero-padding is done, i.e., $N > 2M$. Recall that the original spatial domain image is of dimension $M \times M$ pixels. It is zero-padded such that the 2D-DFT gives a frequency domain image of dimension $N \times N$ pixels. The detailed algorithm is given in Algorithm 1.

The main idea behind Algorithm 1 is that if the map \mathcal{T} is a contraction mapping, by Banach's contraction mapping

Algorithm 1: Algorithm using one-bit noisy recordings of the 2D-DFT for signal reconstruction

Input: $(\tilde{X}_R, \mathcal{F}, \varepsilon)$
Output: G

- 1 $\tilde{G}_0 = 0$ ◁ initialization
- 2 **repeat**
- 3 | $\tilde{G}_{k+1} = \mathcal{T}(\tilde{G}_k)$ ◁ Contraction mapping
- 4 **until** k^* such that $\|\tilde{G}_{k^*} - \tilde{G}_{k^*-1}\|_F \leq \varepsilon$
- 5 $G = \mathfrak{F}^{-1}(\tilde{G}_{k^*})$ ◁ Converting to spatial domain

principle, \mathcal{T} has a unique fixed point. Here the complete metric space on which \mathcal{T} is defined is $\mathbb{R}^{N \times N}$. We show in Section IV that for large enough N/M , the fixed point of \mathcal{T} is a good estimate of the real part of the 2D-DFT of the image to be reconstructed. More specifically, we show that the expected MSE between the fixed point of \mathcal{T} and the real part of the 2D-DFT of the original image is $O(M^2/N^2)$. We use Picard's iteration to reach the fixed point of \mathcal{T} , starting from any finite point. We show in Lemma 3 in Appendix A that the convergence of the recursion to the fixed point is guaranteed by choosing the parameter γ as in eq. (7). To obtain a fast convergence to the fixed point, γ is set very close to, but less than $\frac{2}{f_{\max}}$. A denoised version of the required image in the spatial domain can be obtained from an estimate of the real part of its 2D-DFT by computing its 2D-IDFT if there is sufficient zero padding, i.e., $(N > 2M)$.

In Subsection III-B we discuss the second variation of the proposed algorithm, i.e., Algorithm 2, which is used for signal reconstruction from two-bit recordings of its 2D-DFT.

B. Using two-bit recordings of the noisy 2D-DFT phase

Let $\tilde{g}[k_1, k_2] := \tilde{g}_R[k_1, k_2] + j\tilde{g}_I[k_1, k_2] \in \mathbb{C}^{N \times N}$ be the image in the frequency domain and $\tilde{X}[k_1, k_2] := \tilde{X}_R[k_1, k_2] + j\tilde{X}_I[k_1, k_2] \in \mathbb{C}^{N \times N}$ be recorded according to the sampling models (1) and (2). Define the following subset of the set of complex numbers, $\mathbb{S}_c := \{(a + jb) | a, b \in [-255N^2, 255N^2]\}$.

Let operator $\mathcal{Q} : \mathbb{S}_c^{N \times N} \rightarrow \mathbb{S}_c^{N \times N}$ be defined as:

$$\mathcal{Q}(\tilde{g}) := \mathfrak{F}(\text{CLIP}(\text{PROJ}(\mathfrak{F}^{-1}(\tilde{g}))))). \quad (8)$$

Operator \mathcal{Q} is similar to operator \mathcal{P} used in Algorithm 1, but applies to complex matrices. It computes the 2D-IDFT of the frequency domain argument, projects it onto the support region in the spatial domain (PROJ), clips the pixel values to lie in the range $[0, 255]$ (CLIP), and then computes the 2D-DFT to get the output in the frequency domain. Recall that the support region in the spatial domain is given by the pixels other than the zero-padding pixels of the image. The clipping operation, performed within \mathcal{Q} in the spatial domain, ensures that $\mathcal{Z}(\tilde{g})$ is in $\mathbb{S}_c^{N \times N}$ for all \tilde{g} in $\mathbb{S}_c^{N \times N}$. Similar to \mathcal{P} , every operation within \mathcal{Q} is a projection operation and therefore, \mathcal{Q} is a projection operator. By the property of projection operators, \mathcal{Q} is non-expansive with respect to the Frobenius norm. We call this the NON-EXPANSIVE property of \mathcal{Q} .

Define the map $\mathcal{Z} : \mathbb{S}_c^{N \times N} \rightarrow \mathbb{S}_c^{N \times N}$ as:

$$\begin{aligned} \mathcal{Z}(\tilde{g}) = & \quad (9) \\ & \mathcal{Q} \left(\gamma(\tilde{X}_R + j\tilde{X}_I) + \tilde{g} - \gamma \left(\mathcal{F}(\tilde{g}_R) + j\mathcal{F}(\tilde{g}_I) - \frac{1+j}{2} \right) \right), \\ & \gamma \in \left(0, \frac{2}{f_{\max}} \right). \quad (10) \end{aligned}$$

Recall that the function $\mathcal{F} : \mathbb{R}^{N \times N} \rightarrow \mathbb{R}^{N \times N}$ is the cumulative distribution function of the noise and f_{\max} is the maximum value of the noise PDF for x in the region within the bounds of the signal.

Algorithm 2: Algorithm using two-bit noisy recordings of the 2D-DFT for signal reconstruction

Input: $(\tilde{X}_R, \tilde{X}_I, \mathcal{F}, \varepsilon)$
Output: G

- 1 $\tilde{G}_0 = 0$ ◁ initialization
- 2 **repeat**
- 3 | $\tilde{G}_{k+1} = \mathcal{Z}(\tilde{G}_k)$ ◁ Contraction mapping
- 4 **until** k^* such that $\|\tilde{G}_{k^*} - \tilde{G}_{k^*-1}\|_F \leq \varepsilon$
- 5 $G = \mathfrak{F}^{-1}(\tilde{G}_{k^*})$ ◁ Converting to spatial domain

If \mathcal{Z} is a contraction mapping, then by the Banach's contraction mapping theorem, it has a unique fixed point. \mathcal{Z} is defined over the complete metric space $\mathbb{C}^{N \times N}$. In Lemma 5 in Appendix B, we show that \mathcal{Z} is indeed a contraction mapping with the Frobenius norm as the distance metric. We also show in Section IV that this fixed point of \mathcal{Z} is a good estimate of the 2D-DFT of the original image, with the expected MSE of $O(M^2/N^2)$. As in Algorithm 1, we use Picard's iteration to reach the fixed point of \mathcal{Z} . As shown in Lemma 5, the convergence of the recursion in Algorithm 2 is guaranteed by choosing the parameter γ in \mathcal{Z} as in eq. (10).

IV. THEORETICAL RESULT ON THE ERROR IN RECONSTRUCTION

In this section we provide proofs of the bounds on the expected MSE for the two variations of the algorithm given in the previous section. In Subsection IV-A, we give a proof of the error bound for Algorithm 1.

A. Error bound for Algorithm 1

In this sub-section, we give the error convergence result for Algorithm 1 as a function of M/N . Let the original spatial domain image be $g[n_1, n_2]$ and its 2D-DFT be given by $\tilde{g}[k_1, k_2] = \tilde{g}_R[k_1, k_2] + j\tilde{g}_I[k_1, k_2]$. Define $l_R := \mathcal{F}(\tilde{g}_R) - \frac{1}{2}$. Recall that the sign recordings of noisy $\tilde{g}[k_1, k_2]$ are $\tilde{X}_R[k_1, k_2]$. Define $S := \mathcal{P}(\tilde{X}_R)$.

Lemma 1. $\mathbb{E}[\tilde{X}_R] = l_R$ and $\mathbb{E}[S] = \mathcal{P}(l_R)$.

Proof. $\mathbb{E}[\tilde{X}_R] = l_R$ follows from the definition of \tilde{X}_R and the fact that the noise is additive zero-mean and its distribution is symmetric w.r.t. 0 (Assumption 1). Recall that \mathcal{P} performs a series of four operations: $\mathfrak{F}^{-1}()$, PROJ, CLIP, and $\mathfrak{F}()$. When applying CLIP to $\text{PROJ}(\mathfrak{F}^{-1}(\tilde{X}_R))$, the argument

remains unchanged. This is because $\tilde{X}_R[k_1, k_2] \in \{-\frac{1}{2}, \frac{1}{2}\}$ and by the definition of $\mathfrak{F}^{-1}(\cdot)$ in eq. (4), each element of the $\text{PROJ}(\mathfrak{F}^{-1}(\tilde{X}_R))$ is in $[0, 255]$.¹ Therefore, $\mathcal{P}(\tilde{X}_R) = \mathfrak{F}(\text{PROJ}(\mathfrak{F}^{-1}(\tilde{X}_R)))$ and $\mathcal{P}(l_R) = \mathfrak{F}(\text{PROJ}(\mathfrak{F}^{-1}(l_R)))$. See that $\mathfrak{F}(\text{PROJ}(\mathfrak{F}^{-1}(\cdot)))$ is a linear operation, and by the linearity of expectation, we have $\mathbb{E}[S] = \mathcal{P}(\mathbb{E}[\tilde{X}_R]) = \mathcal{P}(l_R)$. \square

Consider the following recursion using the map \mathcal{T} :

$$\tilde{G}_0 = 0, \quad \tilde{G}_{k+1} = \mathcal{T}(\tilde{G}_k).$$

Let the fixed point of this recursive mapping be $\tilde{G}_{\text{one-bit}}$. We now derive a bound on $\frac{1}{N^2} \mathbb{E}[\|\tilde{G}_{\text{one-bit}} - \tilde{g}_R\|_F^2]$, i.e., the mean-squared error in $\tilde{G}_{\text{one-bit}}$ as an estimate of \tilde{g}_R . The following theorem is the main result with respect to Algorithm 1. The required lemmas are in Appendix A.

Theorem IV.1. *The expected MSE for Algorithm 1 is $O(M^2/N^2)$.*

Proof. Recall the definition $S := \mathcal{P}(\tilde{X}_R)$ and the map \mathcal{T} in eq. (6). Consider two recursions, one using γS in \mathcal{T} and having $\tilde{G}_{\text{one-bit}}$ as fixed point and the other using $\gamma \mathcal{P}(l_R)$ in \mathcal{T} and having \tilde{g}_R as fixed point. Note that the first recursion, using γS , corresponds to using one-bit noisy samples of $\tilde{g}_R[k_1, k_2]$, whereas the second recursion, using $\gamma \mathcal{P}(l_R)$, corresponds to using the perfect information of $\tilde{g}_R[k_1, k_2]$. Since the recursion is insensitive to initialization, we start it with 0. Let,

$$\tilde{G}_0 = \tilde{g}_0 = 0,$$

$$\tilde{G}_{k+1} = \mathcal{T}(\tilde{G}_k) = \gamma S + \mathcal{P}\left(\tilde{G}_k - \gamma\left(\mathcal{F}(\tilde{G}_k) - \frac{1}{2}\right)\right), \quad (11)$$

$$\tilde{g}_{k+1} = \gamma \mathcal{P}(l_R) + \mathcal{P}\left(\tilde{g}_k - \gamma\left(\mathcal{F}(\tilde{g}_k) - \frac{1}{2}\right)\right). \quad (12)$$

The distortion in the reconstructed image in the frequency domain is captured in the difference between these two recursions. Consider the following difference,

$$\begin{aligned} \tilde{G}_{k+1} - \tilde{g}_{k+1} &= \\ &\gamma(S - \mathcal{P}(l_R)) + \mathcal{P}\left(\tilde{G}_k - \tilde{g}_k - \gamma\left(\mathcal{F}(\tilde{G}_k) - \mathcal{F}(\tilde{g}_k)\right)\right). \end{aligned}$$

Using the triangle inequality for the Frobenius norm [39],

$$\begin{aligned} \left\|\tilde{G}_{k+1} - \tilde{g}_{k+1}\right\|_F &\leq \gamma \|S - \mathcal{P}(l_R)\|_F \\ &+ \left\|\mathcal{P}\left(\tilde{G}_k - \tilde{g}_k - \gamma\left(\mathcal{F}(\tilde{G}_k) - \mathcal{F}(\tilde{g}_k)\right)\right)\right\|_F. \end{aligned}$$

By the NON-EXPANSIVE property of \mathcal{P} ,

$$\begin{aligned} \left\|\tilde{G}_{k+1} - \tilde{g}_{k+1}\right\|_F &\leq \gamma \|S - \mathcal{P}(l_R)\|_F + \left\|\tilde{G}_k - \tilde{g}_k - \gamma\left(\mathcal{F}(\tilde{G}_k) - \mathcal{F}(\tilde{g}_k)\right)\right\|_F. \end{aligned}$$

By the Lagrange mean value theorem, $\mathcal{F}(\tilde{G}_k) - \mathcal{F}(\tilde{g}_k) = f(c_k)(\tilde{G}_k - \tilde{g}_k)$ for some matrix $c_k \in \mathbb{R}^{N \times N}$ between \tilde{G}_k and \tilde{g}_k such that each entry of c_k is between the corresponding entries of \tilde{G}_k and \tilde{g}_k . Since \tilde{G}_k and \tilde{g}_k are outputs of T , they

are both in the bounded set $\mathbb{S}^{N \times N}$ and therefore c_k is also in $\mathbb{S}^{N \times N}$. Using this, we get

$$\begin{aligned} \left\|\tilde{G}_{k+1} - \tilde{g}_{k+1}\right\|_F &\leq \\ \gamma \|S - \mathcal{P}(l_R)\|_F + \left\|(1 - \gamma f(c_k))\left(\tilde{G}_k - \tilde{g}_k\right)\right\|_F. \end{aligned}$$

Define α as: $\alpha = \|1 - \gamma f\|_{\max}$. Using α , we get

$$\begin{aligned} \left\|\tilde{G}_{k+1} - \tilde{g}_{k+1}\right\|_F &\leq \gamma \|S - \mathcal{P}(l_R)\|_F + \alpha \left\|\tilde{G}_k - \tilde{g}_k\right\|_F, \\ \text{or, } \left\|\tilde{G}_{k+1} - \tilde{g}_{k+1}\right\|_F - \alpha \left\|\tilde{G}_k - \tilde{g}_k\right\|_F &\leq \gamma \|S - \mathcal{P}(l_R)\|_F. \end{aligned}$$

For parameter γ chosen according to eq. (7), we know from Lemma 3 that both recursions in eqs. (11) and (12) converge to their respective fixed points. Thus the following holds,

$$\begin{aligned} \lim_{k \rightarrow \infty} \left\|\tilde{G}_k - \tilde{g}_k\right\|_F - \alpha \left\|\tilde{G}_{k-1} - \tilde{g}_{k-1}\right\|_F &\leq \gamma \|S - \mathcal{P}(l_R)\|_F, \\ \text{or, } (1 - \alpha) \left\|\tilde{G}_{\text{one-bit}} - \tilde{g}_R\right\|_F &\leq \gamma \|S - \mathcal{P}(l_R)\|_F. \end{aligned}$$

Squaring and taking expectation on the previous inequality,

$$\mathbb{E}[\|\tilde{G}_{\text{one-bit}} - \tilde{g}_R\|_F^2] \leq \frac{\gamma^2 \mathbb{E}[\|S - \mathcal{P}(l_R)\|_F^2]}{(1 - \alpha)^2}.$$

Since we want to calculate the expected mean squared error, we average over all entries of the estimated image in the frequency domain. By Lemma 1 and the bound on the variance of S from Lemma 4 in Appendix A, we get

$$\frac{1}{N^2} \mathbb{E}[\|\tilde{G}_{\text{one-bit}} - \tilde{g}_R\|_F^2] \leq \frac{\gamma^2 (M^2/2N^2)}{(1 - \alpha)^2}. \quad (13)$$

See that the addition of AWGN dither noise ensures that $f(x) > 0$ for all x in the region within the bound of the signal. This ensures that for γ chosen via eq. (7), $\alpha < 1$. For example with $\gamma = 1/f_{\max}$ we get $\alpha = 1 - f_{\min}/f_{\max}$. Since the parameters γ and α are independent of the image dimension, the expected MSE in the estimate of $\tilde{g}_R[k_1, k_2]$ is $O(M^2/N^2)$. To obtain an estimate of spatial domain image $g[n_1, n_2]$, we compute the 2D-IDFT of $\tilde{G}_{\text{one-bit}}$. Now we get a $N \times N$ pixels image in the spatial domain which consists of two copies of the required estimate of $g[n_1, n_2]$ of $M \times M$ pixels each, surrounded by zero-padding. We take an average over these two copies to get the final estimate. \square

B. Error bound for Algorithm 2

In this subsection we give the proof for the variation of the algorithm using two-bit recordings of the noisy 2D-DFT. The proof is very similar to that for Algorithm 1. The only major difference is that here we deal with complex numbers instead of real numbers. We need the following definitions:

$$Y := \mathcal{Q}(\tilde{X}_R + j\tilde{X}_I), \quad (14)$$

$$l := \mathcal{F}(\tilde{g}_R) + j\mathcal{F}(\tilde{g}_I) - \frac{1+j}{2}. \quad (15)$$

See that Y is analogous to S in the proof of Theorem (IV.1). γY corresponds to the first term in the map \mathcal{Z} in eq. (9).

Lemma 2. $\mathbb{E}[\tilde{X}] = l$ and $\mathbb{E}[Y] = \mathcal{Q}(l)$.

¹ \tilde{X}_R is pre-processed to preserve symmetry due to which $\mathfrak{F}^{-1}(\tilde{X}_R) \geq 0$.

Proof. The proof is similar to that of Lemma 1. $\mathbb{E}[\tilde{X}] = l$ follows from Assumption 1 on the noise distribution. CLIP does not change $\text{PROJ}(\mathfrak{F}^{-1}(\tilde{X}))$. This is because each element of $\text{PROJ}(\mathfrak{F}^{-1}(\tilde{X}))$ is in $[0, 255]$. Therefore, $\mathcal{Q}(\tilde{X}) = \mathfrak{F}(\text{PROJ}(\mathfrak{F}^{-1}(\tilde{X})))$ and $\mathcal{Q}(l) = \mathfrak{F}(\text{PROJ}(\mathfrak{F}^{-1}(l)))$. Since $\mathfrak{F}(\text{PROJ}(\mathfrak{F}^{-1}(\cdot)))$ is a linear operation, and by the linearity of expectation, we have $\mathbb{E}[Y] = \mathcal{P}(\mathbb{E}[\tilde{X}]) = \mathcal{P}(l_R)$. \square

Consider the following recursion using \mathcal{Z}

$$\tilde{G}^{(0)} = 0, \quad \tilde{G}^{(k+1)} = \mathcal{Z}(\tilde{G}^{(k)}).$$

Let the fixed point of this recursive mapping be $\tilde{G}_{\text{two-bit}}$. We now derive a bound on $\frac{1}{N^2} \mathbb{E}[\|\tilde{G}_{\text{two-bit}} - \tilde{g}\|_F^2]$. The following theorem is the main result with respect to Algorithm 2. The required lemmas are in the Appendix B.

Theorem IV.2. *The expected MSE for Algorithm 2 is $O(M^2/N^2)$.*

Proof. (IV.1). Consider two recursions, one using γY and having $\tilde{G}_{\text{two-bit}}$ as its fixed point and the other using $\mathcal{Q}(l)$, having \tilde{g} as its fixed point. Note that the first recursion uses the two-bit noisy recordings of the 2D-DFT, whereas the second recursion uses the perfect information of the original frequency domain image $\tilde{g}[k_1, k_2]$. Let,

$$\begin{aligned} \tilde{G}^{(0)} &= \tilde{g}^{(0)} = 0, \\ \tilde{G}^{(k+1)} &= \mathcal{Z}(\tilde{G}^{(k)}) = \\ &\gamma Y + \mathcal{Q}\left(\tilde{G}^{(k)} - \gamma\left(\mathcal{F}(\tilde{G}_R^{(k)}) + j\mathcal{F}(\tilde{G}_I^{(k)}) - \frac{1+j}{2}\right)\right), \end{aligned} \quad (16)$$

$$\begin{aligned} \tilde{g}^{(k+1)} &= \\ &\gamma \mathcal{Q}(l) + \mathcal{Q}\left(\tilde{g}^{(k)} - \gamma\left(\mathcal{F}(\tilde{g}_R^{(k)}) + j\mathcal{F}(\tilde{g}_I^{(k)}) - \frac{1+j}{2}\right)\right). \end{aligned} \quad (17)$$

To calculate the distortion, consider the following difference,

$$\begin{aligned} \tilde{G}^{(k+1)} - \tilde{g}^{(k+1)} &= \gamma(Y - \mathcal{Q}(l)) + \mathcal{Q}\left(\tilde{G}^{(k)} - \tilde{g}^{(k)}\right) \\ &\quad - \gamma \mathcal{Q}\left(\mathcal{F}(\tilde{G}_R^{(k)}) + j\mathcal{F}(\tilde{G}_I^{(k)}) - \mathcal{F}(\tilde{g}_R^{(k)}) - j\mathcal{F}(\tilde{g}_I^{(k)})\right). \end{aligned}$$

Using the triangular inequality for Frobenius norm [39],

$$\begin{aligned} \left\|\tilde{G}^{(k+1)} - \tilde{g}^{(k+1)}\right\|_F &\leq \gamma \|Y - \mathcal{Q}(l)\|_F + \left\|\mathcal{Q}\left(\tilde{G}^{(k)} - \tilde{g}^{(k)}\right)\right. \\ &\quad \left. - \gamma \mathcal{Q}\left(\mathcal{F}(\tilde{G}_R^{(k)}) + j\mathcal{F}(\tilde{G}_I^{(k)}) - \mathcal{F}(\tilde{g}_R^{(k)}) - j\mathcal{F}(\tilde{g}_I^{(k)})\right)\right\|_F. \end{aligned}$$

By the NON-EXPANSIVE property of \mathcal{Q} ,

$$\begin{aligned} \left\|\tilde{G}^{(k+1)} - \tilde{g}^{(k+1)}\right\|_F &\leq \gamma \|Y - \mathcal{Q}(l)\|_F + \left\|\left(\tilde{G}^{(k)} - \tilde{g}^{(k)}\right)\right. \\ &\quad \left. - \gamma\left(\mathcal{F}(\tilde{G}_R^{(k)}) + j\mathcal{F}(\tilde{G}_I^{(k)}) - \mathcal{F}(\tilde{g}_R^{(k)}) - j\mathcal{F}(\tilde{g}_I^{(k)})\right)\right\|_F. \end{aligned}$$

By the Lagrange mean value theorem, $\mathcal{F}(\tilde{G}_R^{(k)}) - \mathcal{F}(\tilde{g}_R^{(k)}) = f(a_k)(\tilde{G}_R^{(k)} - \tilde{g}_R^{(k)})$ for some matrix $a_k \in \mathbb{R}^{N \times N}$ between $\tilde{G}_R^{(k)}$ and $\tilde{g}_R^{(k)}$ such that each entry of a_k is between the corresponding entries of $\tilde{G}_R^{(k)}$ and $\tilde{g}_R^{(k)}$. Similarly, $\mathcal{F}(\tilde{G}_I^{(k)}) - \mathcal{F}(\tilde{g}_I^{(k)}) = f(b_k)(\tilde{G}_I^{(k)} - \tilde{g}_I^{(k)})$ for some matrix $b_k \in \mathbb{R}^{N \times N}$ between $\tilde{G}_I^{(k)}$ and $\tilde{g}_I^{(k)}$. Since \tilde{G}_k and \tilde{g}_k are outputs of \mathcal{Q} ,

they are both in the bounded set $\mathbb{S}_c^{N \times N}$ and therefore $a_k + jb_k$ is also in $\mathbb{S}_c^{N \times N}$. Using this:

$$\begin{aligned} \left\|\tilde{G}^{(k+1)} - \tilde{g}^{(k+1)}\right\|_F &\leq \gamma \|Y - \mathcal{Q}(l)\|_F + \\ &\left\|(1 - \gamma f(a_k))(\tilde{G}_R^{(k)} - \tilde{g}_R^{(k)}) + j(1 - \gamma f(b_k))(\tilde{G}_I^{(k)} - \tilde{g}_I^{(k)})\right\|_F. \end{aligned}$$

Using $\alpha = \|1 - \gamma f\|_{\max}$, we get,

$$\begin{aligned} \left\|\tilde{G}^{(k+1)} - \tilde{g}^{(k+1)}\right\|_F &\leq \gamma \|Y - \mathcal{Q}(l)\|_F + \alpha \left\|\left(\tilde{G}_R^{(k)} - \tilde{g}_R^{(k)}\right) + j\left(\tilde{G}_I^{(k)} - \tilde{g}_I^{(k)}\right)\right\|_F, \\ &\leq \gamma \|Y - \mathcal{Q}(l)\|_F + \alpha \left\|\tilde{G}^{(k)} - \tilde{g}^{(k)}\right\|_F, \end{aligned}$$

or,

$$\left\|\tilde{G}^{(k+1)} - \tilde{g}^{(k+1)}\right\|_F - \alpha \left\|\tilde{G}^{(k)} - \tilde{g}^{(k)}\right\|_F \leq \gamma \|Y - \mathcal{Q}(l)\|_F.$$

For parameter γ chosen according to eq. (10), from Lemma 5 we know that both the recursions in eqs. (16) and (17) converge to their respective fixed points. Thus,

$$\begin{aligned} \lim_{k \rightarrow \infty} \left\|\tilde{G}^{(k+1)} - \tilde{g}^{(k+1)}\right\|_F - \alpha \left\|\tilde{G}^{(k)} - \tilde{g}^{(k)}\right\|_F &\leq \gamma \|Y - \mathcal{Q}(l)\|_F, \\ \text{or, } (1 - \alpha) \left\|\tilde{G}_{\text{two-bit}} - \tilde{g}\right\|_F &\leq \gamma \|Y - \mathcal{Q}(l)\|_F. \end{aligned}$$

Squaring and taking expectation on the above inequality,

$$\mathbb{E}[\|\tilde{G}_{\text{two-bit}} - \tilde{g}\|_F^2] \leq \frac{\gamma^2 \mathbb{E}[\|Y - \mathcal{Q}(l)\|_F^2]}{(1 - \alpha)^2}.$$

Since we want to derive the expected mean squared error, we average over all entries of the estimated image. Using Lemma 2 and the bound on the variance of Y from Lemma 6 in Appendix B,

$$\frac{1}{N^2} \mathbb{E}[\|\tilde{G}_{\text{two-bit}} - \tilde{g}\|_F^2] \leq \frac{\gamma^2 (M^2/2N^2)}{(1 - \alpha)^2}. \quad (18)$$

Since the parameters γ and α are independent of the image dimensions M and N , we obtain that the expected MSE in the estimate of $\tilde{g}[k_1, k_2]$ is $O(M^2/N^2)$. To obtain an estimate of the image $g[n_1, n_2]$, we compute the 2D-IDFT of $\tilde{G}_{\text{two-bit}}$. This completes the proof. \square

C. The use of dither

In the sampling model (1) and (2), we mentioned that we add dither to the signal if there is insufficient noise. From the results for Algorithm 1 and Algorithm 2 in (13) and (18) respectively, we see that the error bound depends on γ and α , which depend on the noise distribution. Recall that $\alpha = \|1 - \gamma f\|_{\max}$. Notice that if the noise is not present, then $\alpha = 1$, and the error bound tends to infinity. Further, for a very large noise variance, α is close to 1 and the error bound is large. This justifies the use of dither when the noise is small, and also explains why dither is not required if there is significant noise with the signal.

V. NUMERICAL SIMULATIONS

In this section we provide the numerical validation of the results in Theorems IV.1 and IV.2. We compare Algorithm 1

and Algorithm 2 with two state-of-the-art methods. The first algorithm we consider is the iterative algorithm given in [10]. We call it the ‘COL’ algorithm after the initials of the authors, Curtis, Oppenheim, and Lim. The algorithm COL requires an initial estimate of the 2D-DFT magnitude. As in [10], we use an average of 2D-DFT magnitudes of a large number of natural images to provide this estimate. The other algorithm is derived from the compressed sensing algorithm: *binary iterative hard-thresholding with partial support estimate weighting (BIHT-PSW)* [40]. It is shown in [40] that their algorithm is robust against noise. The algorithm makes use of the knowledge of the support region. In the scenario of this paper, we have complete knowledge of the support in the spatial domain and thus we call it *binary iterative hard-thresholding with support information, or BIHT-SI*. We do not use convex relaxation based methods [24], [25] for the comparison because they are not designed for the relatively high noise variance regime we consider in this paper.

We consider four benchmark images, viz, the cameraman, Lena, peppers, and IEEE logo images of dimensions 128×128 pixels each. Thus, $M = 128$ in this experiment. These four original images are shown in Fig. 2a. The noise is considered to be uncorrelated AWGN of variance $\sigma^2 = 100$. We do not add dither in the experiments.

Experiment 1. In this test, we verify IV.1IV.2 that the expected MSE is asymptotically of order $O(M^2/N^2)$. Here the oversampling ratio is N^2/M^2 for the image. The pixel intensities in the spatial domain are in the range of $[0, 255]$. For natural images, on computing the 2D-DFT, the intensities are much larger for the lower frequencies and smaller for the higher frequencies. The value of the noise variance relative to the pixel intensities is high, as evident from the weak reconstruction performance of the *BIHT-SI* and *COL* despite the use of guided filtering too, as shown in Figs. 2b and 2c.

The results of $\log_{10}(MSE)$ v/s $\log_{10}(N/M)$ for fixed M are shown in Figs. 3a, 3b, 3c, and 3d. The slopes of the curves in Figs. 3a, 3b, 3c, and 3d, corresponding to Algorithm 1, and Algorithm 2 are given in Table I. This verifies Theorems IV.1 and IV.2. Whereas, the slopes corresponding to the other two algorithms, *BIHT-SI* and *COL*, are much smaller and diminishing for larger values of the sampling rate. This implies that their expected MSE doesn’t improve considerably with a higher sampling rate.

Experiment 2. In this test, we compare the quality of image reconstruction by the four algorithms being considered. The PSNR, popular due to its simplicity, is generally not a good metric to compare images [41]. Unlike the human visual system (HVS), the PSNR doesn’t consider structural information such as the edges of the image. The structural similarity index (SSIM) [42] performs better than the PSNR in this regard. However, it fails to measure the badly blurred images. More recent techniques, the Edge Based Structural Similarity (ESSIM) and the Multi-Scale Structural Similarity (MS-SSIM) [43] are designed to improve upon the SSIM in this regard. The MS-SSIM uses dyadic wavelet transform instead of Sobel filtering as in the SSIM. We employ these four metrics: PSNR, SSIM, ESSIM, and MS-SSIM, for the reconstruction quality in this experiment.

For Algorithm 1, *BIHT-SI*, and *COL* the one-bit signal recording is of size 2048×2048 pixels of the noisy real part of the 2D-DFT of the image. For Algorithm 2, the two-bit signal recording is of size 1448×1448 pixels and has one bit each of the noisy real and imaginary parts of the 2D-DFT of the image. Note that $1448 \approx 2048/\sqrt{2}$ and thus, there are equal number of bits of information and a fair comparison between the four algorithms.

The reconstructed images with *COL*, *BIHT-SI*, Algorithm 1, and Algorithm 2 are shown in Figs. 2b, 2c, 2d, and 2e respectively. Tables II, III, IV, and V have the reconstruction quality metrics for these four algorithms². It can be observed that Algorithm 1 and Algorithm 2 have a similar performance and they produce better results than *BIHT-SI* and *COL* on all images by all four metrics of image reconstruction quality.

Image	Lena	IEEE logo	Cameraman	Peppers
Algo. 1	2.03	2.01	2.00	2.04
Algo. 2	2.01	1.97	1.99	2.02

TABLE I: Asymptotic slopes of $\log_{10}(MSE)$ v/s $\log_{10}(N/M)$ plots.

Lena Image ($\sigma^2 = 100$)				
Method	PSNR	SSIM	ESSIM	MS-SSIM
Algorithm 1	37.083	0.972	0.941	0.986
Algorithm 2	39.142	0.978	0.943	0.988
COL	21.800	0.696	0.893	0.882
BIHT-SI	18.426	0.584	0.878	0.786

TABLE II: Comparison of the algorithms on the Lena image on the basis of PSNR, SSIM, ESSIM, and MS-SSIM.

IEEE logo Image ($\sigma^2 = 100$)				
Method	PSNR	SSIM	ESSIM	MS-SSIM
Algorithm 1	37.430	0.989	0.868	0.975
Algorithm 2	37.190	0.991	0.902	0.984
COL	22.202	0.825	0.775	0.923
BIHT-SI	17.880	0.706	0.734	0.821

TABLE III: Comparison of the algorithms on the IEEE logo image on the basis of PSNR, SSIM, ESSIM, and MS-SSIM.

Cameraman Image ($\sigma^2 = 100$)				
Method	PSNR	SSIM	ESSIM	MS-SSIM
Algorithm 1	37.133	0.963	0.906	0.905
Algorithm 2	37.511	0.969	0.905	0.916
COL	20.445	0.602	0.851	0.681
BIHT-SI	16.293	0.450	0.796	0.613

TABLE IV: Comparison of the algorithms on the cameraman image on the basis of PSNR, SSIM, ESSIM, and MS-SSIM.

²Note that the output of the ESSIM and MS-SSIM depends on calibration parameters. We have set these parameters to have good contrast in the results for the four algorithms.



(a) Undistorted original images: Lena, IEEE logo, cameraman, and peppers. All four images are of 128×128 pixels.



(b) Images reconstructed using Algorithm COL with a 2D-DFT of size 2048×2048 and noise variance equal to 100. The images were sharpened and passed through a guided filter after reconstruction using COL to obtain the best possible PSNR.



(c) Images reconstructed using Algorithm BIHT-SI with a 2D-DFT of size 2048×2048 and noise variance equal to 100. The images were sharpened and passed through a guided filter after reconstruction using BIHT-SI to obtain the best possible PSNR.



(d) Images reconstructed using Algorithm 1 with a 2D-DFT of size 2048×2048 and noise variance equal to 100.



(e) Images reconstructed using Algorithm 2 with a 2D-DFT of size 1448×1448 and noise variance equal to 100.

Fig. 2: Simulation results on four benchmark images. The The PSNR and other reconstruction quality metrics are in Tables II, III, IV, and V respectively in the left to right order of the images.

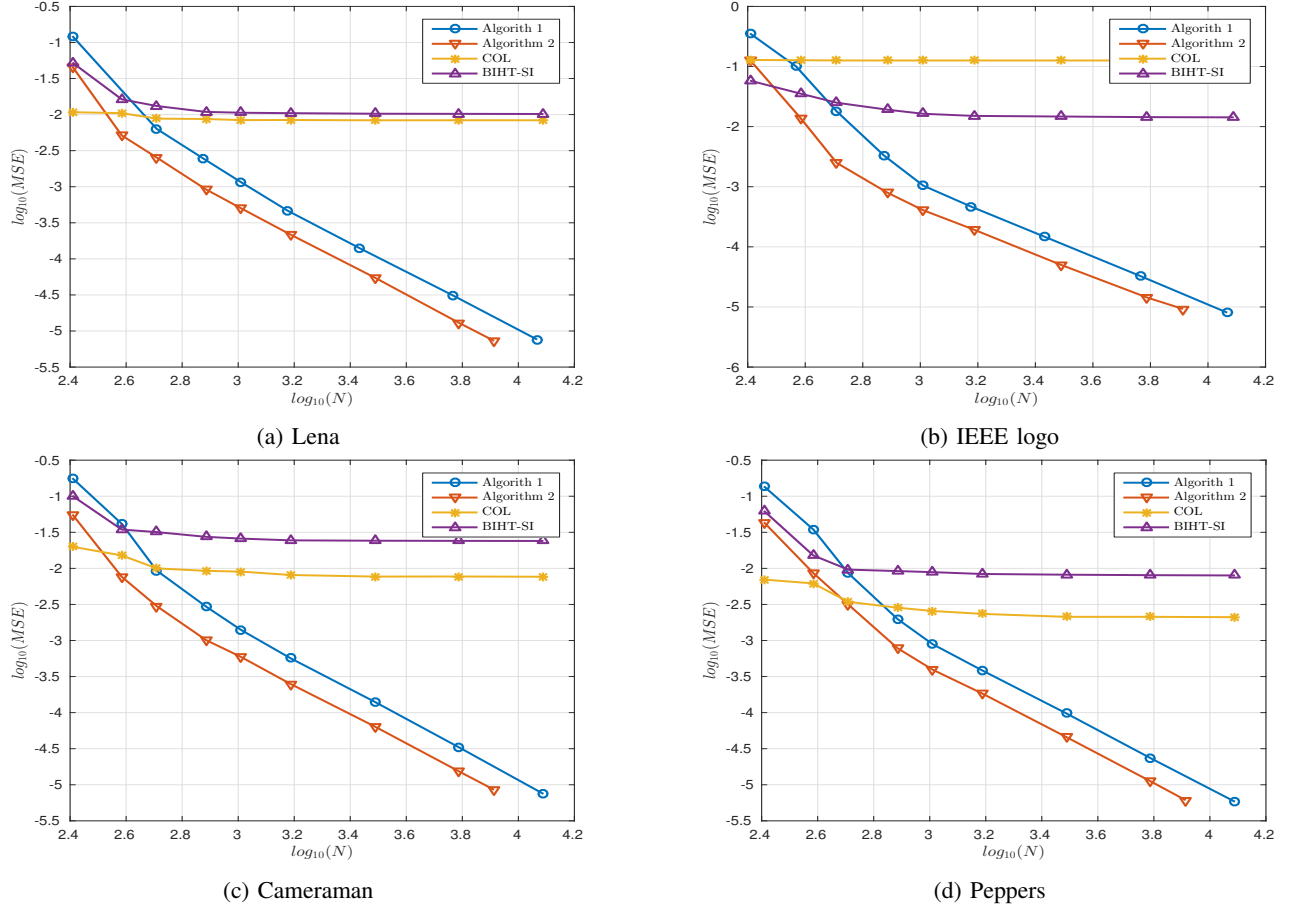


Fig. 3: Plots of $\log(MSE)$ v/s $\log(N)$. Here M is fixed to 128 and N^2/M^2 is the oversampling ratio for the images. The asymptotic slopes of the plots corresponding to Algorithm 1 and 2 are given in Table I.

Peppers Image ($\sigma^2 = 100$)				
Method	PSNR	SSIM	ESSIM	MS-SSIM
Algorithm 1	39.546	0.977	0.961	0.983
Algorithm 2	39.302	0.978	0.965	0.986
COL	26.114	0.797	0.903	0.842
BIHT-SI	19.830	0.592	0.867	0.701

TABLE V: Comparison of the algorithms on the peppers image on the basis of PSNR, SSIM, ESSIM, and MS-SSIM.

VI. CONCLUSIONS

In this paper, we propose two variations of a novel algorithm for the reconstruction of signals using one-bit or two-bit noisy recordings of the 2D-DFT. The signal has zero-mean additive noise of a known symmetric distribution. We use Banach's contraction mapping theorem to provide a recursion that converges to a close estimate of the signal. The expected mean squared error in reconstruction is shown to be $O(M^2/N^2)$, where N^2/M^2 is the oversampling ratio for the image. The result is validated via numerical simulations on four benchmark images. Directions for future work includes developing signal reconstruction algorithms when the noise distributions are not known.

APPENDIX

A. Proof of lemmas for Algorithm 1

Lemma 3. *The map \mathcal{T} is a contraction on the set of real matrices in $\mathbb{S}^{N \times N}$, with the Frobenius distance as the metric.*

Proof. Recall the map \mathcal{T} as given in eq. (6). We need to show that the Frobenius distance between two matrices $\tilde{g}_1 \in \mathbb{S}^{N \times N}$ and $\tilde{g}_2 \in \mathbb{S}^{N \times N}$ decreases on the application of \mathcal{T} ,

$$\|\mathcal{T}(\tilde{g}_1) - \mathcal{T}(\tilde{g}_2)\|_F = \|\mathcal{P}(\tilde{g}_1 - \tilde{g}_2 - \gamma(\mathcal{F}(\tilde{g}_1) - \mathcal{F}(\tilde{g}_2)))\|_F.$$

By the NON-EXPANSIVE property of \mathcal{P} ,

$$\|\mathcal{T}(\tilde{g}_1) - \mathcal{T}(\tilde{g}_2)\|_F \leq \|\tilde{g}_1 - \tilde{g}_2 - \gamma(\mathcal{F}(\tilde{g}_1) - \mathcal{F}(\tilde{g}_2))\|_F.$$

By the Lagrange mean value theorem, $(\mathcal{F}(\tilde{g}_1) - \mathcal{F}(\tilde{g}_2)) = f(c)(\tilde{g}_1 - \tilde{g}_2)$ for some c such that each entry of c is between the corresponding entries of \tilde{g}_1 and \tilde{g}_2 . Thus, we get,

$$\|\mathcal{T}(\tilde{g}_1) - \mathcal{T}(\tilde{g}_2)\|_F \leq \|1 - \gamma f\|_{\max} \|(\tilde{g}_1 - \tilde{g}_2)\|_F.$$

Recall the definition $\alpha := \|1 - \gamma f\|_{\max}$. For \mathcal{T} to be a contraction, we require $0 < \alpha < 1$. This is ensured by restricting γ to $(0, \frac{2}{f_{\max}})$. \square

Lemma 4. *The average variance of $\mathcal{P}(\tilde{X}_R)$ is $O(M^2/N^2)$.*

Proof. Recall that the vectorized form of matrix $g[n_1, n_2]$ is given by $g^v[n]$ and the vectorization operation on a matrix

corresponds to concatenating its columns in order. We know that the 2D-DFT is an orthogonal transform [44]. Therefore, the operation on $g^v[n]$ equivalent to 2D-DFT of $g[n_1, n_2]$ can be given by

$$\tilde{g}^v = NUg^v. \quad (19)$$

Here vector $\tilde{g}^v[k]$ is the vectorized form of $\tilde{g}[k_1, k_2]$. Matrix $U \in \mathbb{C}^{N^2 \times N^2}$ is unitary and has orthonormal columns. Denote the columns of U by u_1, u_2, \dots, u_{N^2} . Similarly, the 2D-IDFT of $\tilde{g}[k_1, k_2]$ can be expressed as an orthogonal transform of $\tilde{g}^v[k]$, given in the terms of the complex conjugate of U as:

$$g^v = \frac{1}{N} U^* \tilde{g}^v. \quad (20)$$

Let the operation on $\tilde{g}^v[k]$, equivalent to the projection operation \mathcal{P} on $\tilde{g}[k_1, k_2]$, be given by $\mathcal{P}^v(\tilde{g}^v)$. In this paper, for an image of size $M \times M$ pixels, a $N \times N$ size 2D-DFT is computed. Here $N > 2M$. The 2D-IDFT of the real-part of the frequency domain image gives two copies of the reconstructed image in the spatial domain. Thus, there are $2M^2$ entries in the support region in the spatial domain. After vectorization, let the indices corresponding to these support region entries be in the set \mathcal{M} . Thus the cardinality of \mathcal{M} is $2M^2$.

By definition $\tilde{X}_R^v[i] \in \{-\frac{1}{2}, \frac{1}{2}\}$. For each $i \in \{1, 2, \dots, N^2\}$, $\text{var}(\tilde{X}_R^v[i]) \leq \frac{1}{4}$. Let $S^v = \mathcal{P}^v(\tilde{X}_R^v)$ be the vectorized form of $\mathcal{P}(\tilde{X}_R)$. Recall that \mathcal{P} consists of computing the 2D-IDFT, followed by projection onto the support set in the spatial domain, clipping to the signal range in the spatial domain, and then computing the 2D-DFT. Its vectorized version \mathcal{P}^v can be given as³:

$$S^v[k] = \mathcal{P}^v(\tilde{X}_R^v) = \sum_{n=1}^{N^2} \left(\sum_{i \in \mathcal{M}} u_i^*[k] u_n[i] \right) \tilde{X}_R^v[n],$$

Since W_R, d_R are i.i.d., the elements of \tilde{X}_R^v are independent,

$$\begin{aligned} \text{var}(S^v[k]) &\leq \sum_{n=1}^{N^2} \left(\sum_{i \in \mathcal{M}} u_i^*[k] u_n[i] \right)^2 \text{var}(\tilde{X}_R^v[n]), \\ &\leq \sum_{n=1}^{N^2} \frac{1}{4} \left(\sum_{i \in \mathcal{M}} u_i^*[k] u_n[i] \right)^2, \\ &= \frac{1}{4} \sum_{n=1}^{N^2} \sum_{i \in \mathcal{M}} \sum_{j \in \mathcal{M}} u_i^*[k] u_j^*[k] u_n[j] u_n[i]. \end{aligned}$$

For unitary matrices, $U^T = U^*$ and thus, $u_n[j] = u_j^*[n]$,

$$\text{var}(S^v[k]) \leq \frac{1}{4} \sum_{n=1}^{N^2} \sum_{i \in \mathcal{M}} \sum_{j \in \mathcal{M}} u_i^*[k] u_j^*[k] u_j^*[n] u_i^*[n].$$

³Recall the proof of Lemma 1, in which we showed that $\mathcal{P}(\tilde{X}_R) = \mathfrak{F}(\text{PROJ}(\mathfrak{F}^{-1}(\tilde{X}_R)))$ since CLIP does not change $\text{PROJ}(\mathfrak{F}^{-1}(\tilde{X}_R))$. This ensures that $\mathcal{P}(\tilde{X}_R)$ is a linear transform of \tilde{X}_R , although \mathcal{P} is not a linear operator in general because of the CLIP operation within it.

By changing the order of summations, we get,

$$\leq \frac{1}{4} \sum_{i \in \mathcal{M}} \sum_{j \in \mathcal{M}} u_i^*[k] u_j^*[k] \delta[i - j] = \frac{1}{4} \sum_{i \in \mathcal{M}} (u_i^*[k])^2.$$

To find the mean variance, we average over k on both sides,

$$\frac{1}{N^2} \sum_{k=1}^{N^2} \text{var}(S^v[k]) \leq \frac{1}{4N^2} \sum_{i \in \mathcal{M}} \sum_{k=1}^{N^2} (u_i^*[k])^2.$$

By the unit norm of the columns of orthonormal matrix U^* and Since \mathcal{M} has $2M^2$ entries,

$$\frac{1}{N^2} \sum_{k=1}^{N^2} \text{var}(S^v[k]) \leq \frac{1}{4N^2} \sum_{i \in \mathcal{M}} 1 = \frac{M^2}{2N^2}.$$

This completes the proof. \square

B. Proof of lemmas for Algorithm 2

Lemma 5. *The map \mathcal{Z} is a contraction on the set of complex matrices in $\mathbb{S}_c^{N \times N}$ with the Frobenius distance as the metric.*

Proof. Recall the map \mathcal{Z} as given in eq. (9). We need to show that the Frobenius distance between two complex matrices $\tilde{g}^{(1)}, \tilde{g}^{(2)} \in \mathbb{S}_c^{N \times N}$ decreases under the application of \mathcal{Z} .

$$\begin{aligned} \left\| \mathcal{Z}(\tilde{g}^{(1)}) - \mathcal{Z}(\tilde{g}^{(2)}) \right\|_F &= \left\| \mathcal{Q}(\tilde{g}^{(1)} - \tilde{g}^{(2)}) \right. \\ &\quad \left. - \gamma \mathcal{Q}(\mathcal{F}(\tilde{g}_R^{(1)}) - \mathcal{F}(\tilde{g}_R^{(2)}) + j\mathcal{F}(\tilde{g}_I^{(1)}) - j\mathcal{F}(\tilde{g}_I^{(2)})) \right\|_F. \end{aligned}$$

By the NON-EXPANSIVE property of \mathcal{Q} ,

$$\begin{aligned} \left\| \mathcal{Z}(\tilde{g}^{(1)}) - \mathcal{Z}(\tilde{g}^{(2)}) \right\|_F &\leq \left\| (\tilde{g}^{(1)} - \tilde{g}^{(2)}) \right. \\ &\quad \left. - \gamma (\mathcal{F}(\tilde{g}_R^{(1)}) - \mathcal{F}(\tilde{g}_R^{(2)}) + j\mathcal{F}(\tilde{g}_I^{(1)}) - j\mathcal{F}(\tilde{g}_I^{(2)})) \right\|_F, \end{aligned}$$

By the Lagrange mean value theorem, as used in Lemma 3,

$$\begin{aligned} &\leq \|1 - \gamma f\|_{\max} \left\| (\tilde{g}_R^{(1)} - \tilde{g}_R^{(2)}) + j(\tilde{g}_I^{(1)} - \tilde{g}_I^{(2)}) \right\|_F, \\ &\leq \|1 - \gamma f\|_{\max} \left\| \tilde{g}^{(1)} - \tilde{g}^{(2)} \right\|_F. \end{aligned}$$

Recall the definition $\alpha = \|1 - \gamma f\|_{\max}$. For \mathcal{Z} to be a contraction map, we require $0 < \alpha < 1$. This is ensured by restricting γ to $(0, \frac{2}{f_{\max}})$. Recall that f_{\max} is the maximum value of $f(x)$ in $x \in (-\infty, \infty)$. \square

Lemma 6. *The average variance of $\mathcal{Q}(\tilde{X})$ is $O(M^2/N^2)$.*

Proof. The proof is similar to that of Lemma 4. Recall that the operator \mathcal{Q} projects the argument to its support region in the spatial domain. For a frequency domain argument, it first computes its 2D-IDFT, then sets the pixels outside the support region to zero, and then finally computes its 2D-DFT. For a 2D-DFT of size $N \times N$ pixels, of an image of size $M \times M$ pixels, there will be $N^2 - M^2$ entries corresponding to the zero-padding, i.e., outside the support region in the spatial domain. Recall that the vectorized form of matrix $g[n_1, n_2]$ is given by $g^v[n]$ and the vectorization operation on a matrix corresponds to concatenating its columns in order. Since the 2D-DFT is an orthogonal transform [44], the operation on

$g^v[n]$ equivalent to 2D-DFT of $g[n_1, n_2]$ can be given as in eq. (19). Similarly, the 2D-IDFT of $\tilde{g}[k_1, k_2]$ can be expressed as an orthogonal transform of $\tilde{g}^v[k]$, as in eq.(20).

Let the operation on $\tilde{g}^v[k]$, equivalent to the projection operation \mathcal{Q} on $\tilde{g}[k_1, k_2]$, be given by $\mathcal{Q}^v(\tilde{g}^v)$. After vectorization, let the indices corresponding to the support region in the spatial domain be in the set \mathcal{M} . Here the cardinality of \mathcal{M} is M^2 .

By definition $\tilde{X}_R^v[i] \in \{-\frac{1}{2}, \frac{1}{2}\}$ and $\tilde{X}_I^v[i] \in \{-\frac{1}{2}, \frac{1}{2}\}$. For each $i \in \{1, 2, \dots, N^2\}$, $\text{var}(\tilde{X}_R^v[i]) \leq \frac{1}{4}$ and $\text{var}(\tilde{X}_I^v[i]) \leq \frac{1}{4}$. Let $Y^v = \mathcal{Q}^v(\tilde{X})$. Since \mathcal{Q} consists of computing 2D-DFT, followed by projection onto the support set and then computing 2D-IDFT, its vectorized version can be given as⁴:

$$Y^v[k] = \sum_{n=1}^{N^2} \left(\sum_{i \in \mathcal{M}} u_i^*[k] u_n[i] \right) \left(\tilde{X}_R^v[n] + j \tilde{X}_I^v[n] \right).$$

Here $u_i, \forall i \in [1, \dots, N^2]$, are the orthonormal columns of \mathcal{U} . Since W_d, d_R, W_I , and d_I are i.i.d., the elements of \tilde{X}_R^v and \tilde{X}_I^v are independent. Therefore,

$$\begin{aligned} \text{var}(Y^v[k]) &\leq \sum_{n=1}^{N^2} \left(\sum_{i \in \mathcal{M}} u_i^*[k] u_n[i] \right)^2 \left(\text{var}(\tilde{X}_R^v[n]) + \text{var}(\tilde{X}_I^v[n]) \right), \\ &= \sum_{n=1}^{N^2} \left(\frac{1}{4} + \frac{1}{4} \right) \left(\sum_{i \in \mathcal{M}} u_i^*[k] u_n[i] \right)^2, \\ &= \frac{1}{2} \sum_{n=1}^{N^2} \sum_{i \in \mathcal{M}} \sum_{j \in \mathcal{M}} u_i^*[k] u_j^*[k] u_n[j] u_n[i]. \end{aligned}$$

Since \mathcal{U} is a unitary matrices, $\mathcal{U}^T = \mathcal{U}^*$, $u_n[j] = u_j^*[n]$, then

$$\text{var}(Y^v[k]) \leq \frac{1}{2} \sum_{n=1}^{N^2} \sum_{i \in \mathcal{M}} \sum_{j \in \mathcal{M}} u_i^*[k] u_j^*[k] u_j^*[n] u_i^*[n].$$

Changing the order of summations,

$$\leq \frac{1}{2} \sum_{i \in \mathcal{M}} \sum_{j \in \mathcal{M}} u_i^*[k] u_j^*[k] \delta[i - j] = \frac{1}{2} \sum_{i \in \mathcal{M}} (u_i^*[k])^2.$$

Being interested in the mean variance, we average over k ,

$$\frac{1}{N^2} \sum_{k=1}^{N^2} \text{var}(Y^v[k]) \leq \frac{1}{2N^2} \sum_{i \in \mathcal{M}} \sum_{k=1}^{N^2} (u_i^*[k])^2.$$

By the unit norm of columns of orthonormal matrix \mathcal{U}^* and since \mathcal{M} has M^2 entries,

$$\frac{1}{N^2} \sum_{k=1}^{N^2} \text{var}(Y^v[k]) \leq \frac{1}{2N^2} \sum_{i \in \mathcal{M}} 1 = \frac{M^2}{2N^2}.$$

This completes the proof. \square

⁴Recall the proof of Lemma 2, in which we showed that $\mathcal{Q}(\tilde{X}) = \mathfrak{F}(\text{PROJ}(\mathfrak{F}^{-1}(\tilde{X})))$ since CLIP does not change $\text{PROJ}(\mathfrak{F}^{-1}(\tilde{X}))$. This ensures that $\mathcal{Q}(\tilde{X})$ is a linear transform of \tilde{X} , although \mathcal{Q} is not a linear operator in general because of the CLIP operation which is a part of \mathcal{Q} .

REFERENCES

- [1] A. V. Oppenheim, J. S. Lim, and S. R. Curtis, "Signal synthesis and reconstruction from partial Fourier-domain information," *JOSA*, vol. 73, no. 11, pp. 1413–1420, 1983.
- [2] J. R. Fienup, "Phase retrieval algorithms: a personal tour," *Applied optics*, vol. 52, no. 1, pp. 45–56, 2013.
- [3] W. Saxton, *Computer techniques for image processing in electron microscopy*. Academic Press, 2013, vol. 10.
- [4] G. N. Ramachandran, G. N. Ramachandran, and R. Srinivasan, *Fourier methods in crystallography*. John Wiley & Sons, 1970.
- [5] E. J. Candes, T. Strohmer, and V. Voroninski, "Phaselift: Exact and stable signal recovery from magnitude measurements via convex programming," *Communications on Pure and Applied Mathematics*, vol. 66, no. 8, pp. 1241–1274, 2013.
- [6] K. Huang, Y. C. Eldar, and N. D. Sidiropoulos, "Phase retrieval from 1d Fourier measurements: Convexity, uniqueness, and algorithms," *IEEE Transactions on Signal Processing*, vol. 64, no. 23, pp. 6105–6117, 2016.
- [7] V. Kishore and C. S. Seelamantula, "Wirtinger flow algorithms for phase retrieval from binary measurements," in *IEEE International Conference on Acoustics, Speech and Signal Processing*, 2020.
- [8] S. Mukherjee and C. S. Seelamantula, "Phase retrieval from binary measurements," *IEEE Signal Processing Letters*, 2018.
- [9] Y. Li and A. Kurkjian, "Arrival time determination using iterative signal reconstruction from the phase of the cross spectrum," *IEEE Transactions on Acoustics, Speech, and Signal Processing*, vol. 31, no. 2, pp. 502–504, 1983.
- [10] S. Curtis, A. Oppenheim, and J. Lim, "Signal reconstruction from Fourier transform sign information," *IEEE transactions on acoustics, speech, and signal processing*, vol. 33, no. 3, pp. 643–657, 1985.
- [11] X. Tang, Y. Yuan, and Y. Wang, "Image reconstruction from one-bit phase information (obpi) with specified histogram constraint," in *IEEE International Symposium on Circuits and Systems*, 1990, pp. 755–758.
- [12] I. Lyuboshenko and A. Akhmetshin, "Stable signal and image reconstruction from noisy Fourier transform phase," *IEEE transactions on signal processing*, vol. 47, no. 1, pp. 244–250, 1999.
- [13] D. Thomas and M. Hayes, "Procedures for signal reconstruction from noisy phase," in *IEEE International Conference on Acoustics, Speech, and Signal Processing*, vol. 9, 1984, pp. 618–621.
- [14] R. Gray, "Oversampled sigma-delta modulation," *IEEE Transactions on Communications*, vol. 35, no. 5, pp. 481–489, 1987.
- [15] E. Masry, "The reconstruction of analog signals from the sign of their noisy samples," *IEEE Transactions on Information Theory*, vol. 27, no. 6, pp. 735–745, 1981.
- [16] T. Thong and J. McNames, "Nonlinear reconstruction of over-sampled coarsely quantized signals," in *The 45th Midwest Symposium on Circuits and Systems*, vol. 2. IEEE, 2002.
- [17] I. Daubechies and R. DeVore, "Approximating a bandlimited function using very coarsely quantized data: A family of stable sigma-delta modulators of arbitrary order," *Annals of mathematics*, vol. 158, no. 2, pp. 679–710, 2003.
- [18] A. Kumar and V. M. Prabhakaran, "Estimation of bandlimited signals from the signs of noisy samples," in *IEEE International Conference on Acoustics, Speech and Signal Processing*, 2013, pp. 5815–5819.
- [19] Z. Cvetkovic and I. Daubechies, "Single-bit oversampled a/d conversion with exponential accuracy in the bit-rate," in *Data Compression Conference, 2000. Proceedings. DCC 2000*. IEEE, 2000, pp. 343–352.
- [20] S. Khobahi, N. Naimipour, M. Soltanalian, and Y. C. Eldar, "Deep signal recovery with one-bit quantization," in *2019 IEEE International Conference on Acoustics, Speech and Signal Processing*, 2019.
- [21] S. Bender, M. Dörpinghaus, and G. Fettweis, "On the spectral efficiency of bandlimited 1-bit quantized awgn channels with runlength-coding," *IEEE Communications Letters*, 2020.
- [22] Z. Shao, L. T. N. Landau, and R. C. de Lamare, "Channel estimation using 1-bit quantization and oversampling for large-scale multiple-antenna systems," in *IEEE International Conference on Acoustics, Speech and Signal Processing (ICASSP)*, 2019, pp. 4669–4673.
- [23] M. Goyal and A. Kumar, "Estimation of bandlimited signals on graphs from single bit recordings of noisy samples," in *2018 26th European Signal Processing Conference (EUSIPCO)*. IEEE, 2018, pp. 902–906.
- [24] P. T. Boufounos and R. G. Baraniuk, "1-bit compressive sensing," in *IEEE Conference on Information Sciences and Systems*, 2008.
- [25] A. Zymnis, S. Boyd, and E. Candes, "Compressed sensing with quantized measurements," *IEEE Signal Processing Letters*, vol. 17, no. 2, pp. 149–152, 2010.

- [26] C. Xu and L. Jacques, "Quantized compressive sensing with rip matrices: The benefit of dithering," *Information and Inference: A Journal of the IMA*, 2018.
- [27] L. Jacques, J. N. Laska, P. T. Boufounos, and R. G. Baraniuk, "Robust 1-bit compressive sensing via binary stable embeddings of sparse vectors," *IEEE Transactions on Information Theory*, vol. 59, no. 4, pp. 2082–2102, 2013.
- [28] M. P. Friedlander, H. Jeong, Y. Plan, and O. Yilmaz, "NBIHT: an efficient algorithm for 1-bit compressed sensing with optimal error decay rate," *arXiv preprint arXiv:2012.12886*, 2020.
- [29] P. T. Boufounos, "Angle-preserving quantized phase embeddings," in *Wavelets and Sparsity XV*, vol. 8858. International Society for Optics and Photonics, 2013.
- [30] —, "Sparse signal reconstruction from phase-only measurements," in *Proc. Int. Conf. Sampling Theory and Applications*. Citeseer, 2013.
- [31] L. Jacques and T. Feuilleux, "The importance of phase in complex compressive sensing," *arXiv preprint arXiv:2001.02529*, 2020.
- [32] G. A. Seber and A. J. Lee, *Linear regression analysis*. John Wiley & Sons, 2012, vol. 329.
- [33] V. K. Goyal, M. Vetterli, and N. T. Thao, "Quantized overcomplete expansions in ir/sup n: analysis, synthesis, and algorithms," *IEEE Transactions on Information Theory*, vol. 44, no. 1, pp. 16–31, 1998.
- [34] A. Ai, A. Lapanowski, Y. Plan, and R. Vershynin, "One-bit compressed sensing with non-gaussian measurements," *Linear Algebra and its Applications*, vol. 441, pp. 222–239, 2014.
- [35] Y. Plan and R. Vershynin, "One-bit compressed sensing by linear programming," *Communications on Pure and Applied Mathematics*, vol. 66, no. 8, pp. 1275–1297, 2013.
- [36] S. So and K. K. Paliwal, "Reconstruction of a signal from the real part of its discrete Fourier transform [tips & tricks]," *IEEE Signal Processing Magazine*, vol. 35, no. 2, pp. 162–174, 2018.
- [37] S. Bahmani, P. T. Boufounos, and B. Raj, "Robust 1-bit compressive sensing via gradient support pursuit," *arXiv preprint arXiv:1304.6627*, 2013.
- [38] M. F. Wagdy, "Effect of various dither forms on quantization errors of ideal a/d converters," *IEEE Transactions on Instrumentation and Measurement*, vol. 38, no. 4, pp. 850–855, 1989.
- [39] E. Kreyszig, *Introductory functional analysis with applications*. Wiley New York, 1989, vol. 1.
- [40] P. North and D. Needell, "One-bit compressive sensing with partial support," in *2015 IEEE 6th International Workshop on Computational Advances in Multi-Sensor Adaptive Processing*, 2015, pp. 349–352.
- [41] G.-H. Chen, C.-L. Yang, L.-M. Po, and S.-L. Xie, "Edge-based structural similarity for image quality assessment," in *IEEE International Conference on Acoustics Speech and Signal Processing Proceedings*, 2006.
- [42] Z. Wang, A. C. Bovik, H. R. Sheikh, and E. P. Simoncelli, "Image quality assessment: from error visibility to structural similarity," *IEEE Transactions on Image Processing*, vol. 13, no. 4, pp. 600–612, 2004.
- [43] Z. Wang, E. P. Simoncelli, and A. C. Bovik, "Multiscale structural similarity for image quality assessment," in *The Asilomar Conference on Signals, Systems Computers*, vol. 2, 2003, pp. 1398–1402 Vol.2.
- [44] A. K. Jain, *Fundamentals of digital image processing*. Englewood Cliffs, NJ: Prentice Hall, 1989.